

October 4th, 2015

Dear Editor,

Attached is our 2nd revised manuscript, “Phytoplankton dynamics driven by vertical nutrient fluxes during the spring inter-monsoon period in the northeastern South China Sea” by Li Q.P., Dong Y., and Wang Y.

We are grateful to the comments from the reviewers. We have addressed all the reviewer’s points (**highlighted by blue color**) in the revised manuscript, and the detail of our point-to-point response to the reviewer’s comments follows. We hope that you will now find our manuscript suitable for publication.

Sincerely yours,

Qian Li
South China Sea Institute of Oceanology
Chinese Academy of Sciences, Guangzhou, China
Email: qianli@scsio.ac.cn

Response to reviewer

1. At the abstract, the conclusion was introduced from the pigment analysis and so the result of pigment analysis is important, however, the methods and results of pigment analysis were not described in the text. The authors described “diatom-rich” and “picoplankton” dominant. How they concluded them? By the pigment analysis, the size of the phytoplankton cannot be clear.

Response: We have decided to remove this part of the abstract related to pigment data in the revised manuscript, as we think it is not directly related to the focus of our paper and as the pigment data of the cruise will be reported in an individual paper by another group of scientists.

2. The authors described that the station B is the representative station near the Dongsha. However, this station was the edge eddies, and the physical properties must vary at meso and/or submeso-scale. The authors pointed that the eddies are usually formed in this area, but the nutrient flux must vary in the cyclonic and anticyclonic eddies and/or the edge of the eddies. Such a discussion was not seen in the text. Therefore, I recognized that the description “the elevated nutrient flux near the Dongsha Island...” is over-discussion.

Response: discussion of the effect of eddies on vertical nutrient transport has been provided in the revised manuscript. Region of the southeast Dongsha Islands has been well documented for its intense turbulent mixing because of internal waves and eddies (e.g. Lien et al., 2005; Chow et al., 2008). The observed high vertical diffusivity and nitrate flux at station B during our field study may be contributed by physical dynamics associated with eddy-eddy interactions (Fig. 2a). The frontal zones at the edge of eddies are often places of increased vertical mixing (Klein and Lapeyre 2009; Li et al., 2012), though the eddy-induced vertical fluxes may vary substantially between cyclonic, anticyclonic and mode-water eddies (McGillicuddy et al., 2007).

3. In the Materials and methods, Li and Hansell 2008 DSRII was referred as the nutrient analysis method, however, in that paper, the high sensitive analysis methods using the 2-m long cells are described, but the “standard” methods are not described. In usual, an AA3 analyzer are equipped ~10 cm cell. I cannot understand that the nutrient concentration was measured by long cells with dilution or by short cells. These were concerned with the accuracy; the authors did not show the detection limits but described as “Measurement errors of nutrients at depths during the field study could be negligible as the concentrations are considerably higher than the detection limits of the analytical methods”.

Response: In the revised manuscript, details of nutrient measurements have been provided in the method section 2.1. Nutrient concentrations below the euphotic zone are measured by AA3 analyzer with 10cm cells. We also used the long-path colorimetric method (Li et al., 2008; Li and Hansell 2008) to measure the low concentrations of nitrate plus nitrite and phosphate by incorporating a 50cm liquid waveguide cell to AA3 with detection limits of 0.02 uM and 0.01 uM, respectively

4. Also in the M&M, the definition of the euphotic layer and/or type of the optical sensor was not described. The authors replied “the PAR is measured during the cruises”, but I cannot see the information of them at this section.

Response: information about optical sensor and the definition of euphotic zone has been added to the method section 2.1.

5. The regression line of Figure 7 was the other problem. The authors relied that “regression line is

automatically generated by excel, we need to remove the line between 0-0.25, as it won't have any impacts on our results." At first, the range of the regression line can be changed in excel, and so this response was unacceptable. And then, is there no impact? The authors did not describe that the dilution series of 0% is not prepared at station B in the text, while it was described in the response. The readers cannot judge that the dilution of 0% was prepared or not because of the inconsistent with the text and figures.

Response: Fine. We have removed the regression line between 0-0.25 and we have clearly pointed out that the sample 0% unfiltered seawater was not taken at station B in the method section 2.4.

6. L448 "The integrated phytoplankton chlorophyll-a biomass during the transect study showed a positive correlation with upward nitrate flux ($r^2=0.35$) when station C9 was not included (Table 1), supporting the important role of bottom-up control on phytoplankton production in our study area (Chen 2005)." The authors responded the r value is sufficient, however, based on the result of the regression analysis, the p value of the slope is 0.09, which is not significant (in addition, the r^2 value was 0.34 in my calculation based on the data Table 1 by Microsoft excel). Therefore, I cannot agree with this discussion which was very important for the conclusion of this manuscript.

Response: We agree with the reviewer that the correlation is not significant. Correlation between $[Chl \cdot dz]$ and J_{total} will be influenced by many factors including phytoplankton net growth rate, nitrogen to chlorophyll ratio, and isopycnal inputs. The regression can be improved ($[Chl \cdot dz] = 16.75 \times J_{total} + 7.7, r^2 = 0.58, p = 0.014$) if we exclude station C6, which is near the top of the shelf slope. In the revised manuscript, the sentence has been rewritten as "For the deep-water stations including the offshore pelagic zone (C7-C10) and the water intrusion zone (C11-C13), the integrated chlorophyll-a biomass during the transect study shows a positive correlation with the upward nitrate flux ($[Chl \cdot dz] = 16.75 \times J_{total} + 7.7, r^2 = 0.58, p = 0.014$) when stations C9 is not included (Table 1), supporting the important role of bottom-up control on phytoplankton production in our study area (Chen 2005)."'

7. [Specific Comments]
L282 May 14th -16th, 2015

Response: done. 2015 has been changed to 2014

8. L297 "surface chlorophyll patches (~0.3 $\mu\text{g L}^{-1}$) found between ..." At first, the patch means patchy increase? Then the surface chlorophyll a concentration ~0.3 $\mu\text{g L}^{-1}$ was observed at C11, however, at the other stations, the concentration seems to be <0.2 $\mu\text{g L}^{-1}$. What does this sentence mean?

Response: In the revised manuscript, we have clarified that it is the patch of high surface chlorophyll at C11.

9. L308 "The observed uplift of isopycnals as well as the depths of chlorophyll maximum and nutricline at the shelf station C6 and the offshore station C12" As I pointed in the previous review, the subsurface chlorophyll maximum at C8, C9, C10 seemed to be the same depth with C6. Why these stations were ignored?

Response: We have included C8, C9, and C10 in the revised manuscript.

10. L311 "there were substantially higher nutrient concentrations and nutrient gradients at depths of ~200 m ... for both stations C9 and C11 in the offshore regions" The silicate and phosphate concentration was actually elevated, but the nitrate concentration at C11 was the same level with C10.

Please describe accurately, and why the nitrate concentration was not elevated at C10?

Response: The sentence has been rewritten to clearly state that concentrations of phosphate and silicate at 200m were substantially higher in C9 and C11. “why the nitrate concentration was *not* elevated at C10?” I cannot follow the logic of the reviewer here, as both silicate and phosphate at C10 are lower than C11. Anyway, we should not expect the distributions of nitrate, phosphate, and silicate to be exactly the same in seawater.

11. L317 “as horizontal nutrient gradients within euphotic zone are considerably lower than the vertical gradient.” The horizontal advection of eutrophic water cannot be discussed by the only horizontal gradient. The current velocity is also important factor of the horizontal flux. Thus, this discussion is incorporate.

Response: We agree with the reviewer on this point. We have removed the comparison between vertical and horizontal advects.

12. Figure 2c the unit was wrong.

Response: The scale of colorbar in figure 2c has been fixed in the revised manuscript.

13. Figure 6 As I pointed in the previous review, the presentation of the gradient of nutrient concentration was not correct. Authors replied that “Nutrient gradients are calculated from nutrient concentrations. They should have the same depths.” Then, for example, the gradient at 100 m depth indicated from where to where? From 75m to 100 m or from 100 m to 150 m? The nutrient gradient is the depth-average values, isn’t it? The averaged depth was really 100 m depth?

Response: the vertical gradient of nutrient at the depth of Z_i (with a nutrient concentration of C_i) is approximately calculated by $(C_{i+1}-C_i)/(Z_{i+1}-Z_i)$ with C_{i+1} the nutrient concentration at depth Z_{i+1} immediately next to Z_i . We have clarified this in the revised manuscript.

14. Figure 7b The label of the Y-axis was wrong.

Response: the unit should be “Net growth rate [d-1]” and this has been fixed in the revised manuscript.

1 **Phytoplankton dynamics driven by vertical nutrient fluxes during the spring**
2 **inter-monsoon period in the northeastern South China Sea**

3

4 Qian P. Li^{*}, Yuan Dong, Yanjun Wang

5 South China Sea Institute of Oceanology, Chinese Academy of Sciences, Guangzhou,
6 China

7

8

9 Submitted to Biogeosciences on March 27, 2015

10 Revised July 29, 2015

11 2nd revised October 5, 2015

12

13 *Correspondence to: qianli@scsio.ac.cn

14 **Abstract**

15 A field survey from the coastal ocean zones to the offshore pelagic zones of the
16 northeastern South China Sea (nSCS) was conducted during the inter-monsoon period
17 of May 2014 when the region was characterized by prevailing low-nutrient conditions.
18 Comprehensive field measurements were made for not only hydrographic and
19 biogeochemical properties but also phytoplankton growth and microzooplankton
20 grazing rates. We also performed estimations of the vertical turbulent diffusivity and
21 diffusive nutrient fluxes using a Thorpe-scale method and the upwelling nutrient
22 fluxes by Ekman pumping using satellite-derived wind stress curl. Our results suggest
23 that phytoplankton chlorophyll patchiness in the nSCS during the study period is
24 largely controlled by vertical nutrient fluxes with combined contributions from both
25 turbulent diffusion and curl-driven upwelling. Our results also reveal the generally
26 increasing role of turbulent diffusion but decreasing role of curl-driven upwelling on
27 vertical transport of nutrients from the coastal ocean zones to the offshore pelagic
28 zones in the nSCS. [Elevated nutrient fluxes observed near Dongsha Islands were](#)
29 [found to support high new production leading to net growth of phytoplankton](#)
30 [community, whereas the low nutrient fluxes near southwest Taiwan had resulted in a](#)
31 [negative net community growth leading to decline of a surface phytoplankton bloom.](#)

32 **1. Introduction**

33 Nutrient fluxes from below the euphotic zone are essential for phytoplankton
34 primary production in the surface ocean (Eppley and Peterson, 1979), while the
35 mechanisms regulating those fluxes are still inadequately understood in the
36 northeastern South China Sea (nSCS), particularly during the spring intermonsoon
37 period. Wind-driven coastal upwelling, river discharge, and inter-shelf nutrient
38 transport were important mechanisms supplying nutrients to the euphotic zone of the
39 nSCS (Liu et al., 2002; Gan et al., 2010; Han et al., 2013), while their contributions to
40 primary production were mostly limited to coastal regions as these nutrients would be
41 mostly utilized in the coastal waters before reaching the large area of the nSCS.
42 Kuroshio intrusion would dilute the nSCS waters with the low nutrient North Pacific
43 waters (Farris and Wimbush. 1996), which appeared to be much weaker during
44 April-September (Centurioni et al., 2004). Contribution of nitrogen fixation to new
45 production of the nSCS was generally negligible compared to the nitrate-based new
46 production (Chen et al., 2005; Bombar et al., 2010). Atmospheric deposition of
47 anthropogenic nitrogen could support up to ~20% of the annual new production in the
48 nSCS exceeding those from riverine inputs (Kim et al., 2014). But its contribution
49 would be much less during the spring inter-monsoon season as the reduced rate of
50 atmospheric deposition (Lin et al., 2009).

51 Diapycnal mixing by turbulent dissipation was recently found to be important for
52 the supply of new nitrogen in the nSCS, where the vertical turbulent diffusivities were
53 an order of magnitude higher than the adjacent West Pacific Ocean (Tian et al., 2009;
54 Liu and Lozovatsky 2012; Yang et al., 2014). It was also suggested that
55 phytoplankton blooms off the west coast of the nSCS could be induced by wind stress
56 curl-driven upwelling during the spring inter-monsoon season (Wang and Tang 2014),
57 which would cause a local uplift of isopycnals leading to nutrient injection into the
58 euphotic zone with subsequent changes of community structure and productivity
59 (Rykaczewski and Checkley 2008; Li et al., 2015). By modifying the surface wind
60 stress and wind stress curl via air-sea coupling, the eddy-induced Ekman pumping
61 (Gaube et al., 2013) was important for phytoplankton production in the nSCS during
62 the inter-monsoon transition period (Lin et al., 2010). As both intermittent turbulent
63 diffusion and wind-driven Ekman pumping affect the vertical transport of nutrients on
64 temporal scales similar to the generation time of phytoplankton, they will have large
65 influences on plankton dynamics of the upper ocean (Cullen et al., 2002). It is

66 therefore important to investigate the roles of these two mechanisms in driving the
67 variability of phytoplankton biomass and primary production in the large area of the
68 nSCS.

69 Spatial distribution of phytoplankton at sea is a result of complex interactions
70 between physical and biological processes (Davis et al., 1991; Abraham 1998). In
71 addition to the vertical nutrient fluxes, phytoplankton biomass and productivity of the
72 nSCS are influenced by growth-grazing dynamics (Chen 2005; Huang et al., 2011;
73 Zhou et al., 2011; Chen et al., 2013). Shifts in the dominance of phytoplankton
74 species in the western South China Sea were believed to be driven by a close coupling
75 of the mortality rates of different phytoplankton groups via common grazers such as
76 nanoflagellates (Chen et al., 2009). There was on average ~61% of phytoplankton
77 growth lost to microzooplankton grazing in coastal upwelling regions of the nSCS in
78 response to increased nutrient fluxes, whereas growth and grazing mortality rates
79 were mostly balanced on the shelf and shelf break areas without upwelling events
80 (Huang et al., 2011). It was also suggested that the balance of phytoplankton growth
81 and microzooplankton grazing in the pelagic nSCS could be perturbed by physical
82 disturbances such as eddies, fronts, and typhoons, leading to large deviations of
83 planktonic ecosystem from the steady state (Zhou et al., 2011; Chen et al., 2013).

84 Here, we present results of a field survey from the coastal ocean zones to the
85 offshore pelagic zones in the nSCS conducted during the spring inter-monsoon
86 transition of May 2014, when the region was characterized by prevailing low nutrient
87 conditions as a result of weak and variable winds (Lin et al., 2010). Comprehensive
88 measurements were made for hydrographic and biogeochemical properties, as well as
89 biological rates including phytoplankton growth and grazing rates and net nutrient
90 consumption rates. We also performed estimations of the vertical turbulent diffusivity
91 and diffusive nutrient fluxes using a Thorpe-scale method (Gargett and Garner 2008;
92 Li et al., 2012) and the upwelling nutrient fluxes by Ekman pumping using
93 satellite-derived wind stress curl (Gill 1982; Risien and Chelton 2008). In
94 synthesizing these field data, the focus of this paper are to (1) investigate the spatial
95 patterns of vertical nutrient fluxes in the nSCS, (2) determine the relative roles of
96 turbulent diffusion and Ekman pumping to vertical transport of nutrients in the upper
97 ocean, and (3) understand the linkage between vertical nutrient fluxes and
98 phytoplankton dynamics in the nSCS during the spring inter-monsoon period.

99

100 **2. Materials and methods**

101 **2.1. Site description, field sampling, and measurements**

102 There are typically high nutrients in the coastal regions of the nSCS due to river
103 discharge, inter-shelf transport, and upwelling and mixing (Gan et al., 2010), in
104 contrast to the oligotrophic low-latitude offshore regions with strong stratification.
105 The nSCS is also strongly influenced by Kuroshio intrusion through the Luzon Strait
106 (Farris and Wimbush 1996). The intruded Kuroshio waters with higher temperature
107 and salinity but lower nutrients are often transported westward via eddies and Ekman
108 advection (Centurioni et al., 2004) influencing the large area of the nSCS on seasonal
109 time-scales.

110 A field survey of the nSCS (Fig. 1) was conducted during May 2014 aboard the
111 *R/V Shiyuan III* of the South China Sea Institute of Oceanology. From May 14th to May
112 16th, 2014, a transect from the coastal waters near Shantou to the offshore waters near
113 the Luzon Strait was comprehensively sampled to investigate the spatial patterns of
114 hydrographic and biogeochemical properties of the nSCS. Station S₁ (22°N, 119.5°E)
115 was chosen as a reference time-series station with continuous CTD sampling of 13
116 casts within 24 hours (start: 10:00 am, May 18th, 2014). Stations A (21.9°N, 120°E
117 with a bottom depth of 1547 m) near the southwest of Taiwan and station B (20.5°N,
118 117°E with a bottom depth of 607 m) in the southeast of Dongsha Islands were
119 selected for dilution experiments to quantify phytoplankton growth and
120 microzooplankton grazing rates.

121 Discrete seawater samples at depths of 0 m, 25 m, 50 m, 75 m, 100 m, 200 m, 300
122 m, 500 m, and 700 m were collected using a SeaBird SBE 9/11 CTD rosette water
123 sampler system, providing high resolution hydrographic measurements of the upper
124 water column with internal pressure, conductivity, and temperature sensors. We define
125 euphotic zone as the layer above 1% of surface Photosynthetically Active Radiation
126 (PAR), measured by a PAR sensor (Biospherical Instrument, Inc.). After inline
127 filtrations from the PVC Niskin bottles through 0.8 µm Nuclepore filters, seawater
128 samples for nutrients were frozen immediately and stored in a refrigerator until final
129 analyses after the cruise. For chlorophyll-*a* sampling, 500 ml of seawater was gently
130 filtered (<50 mmHg) through a GF/F (Whatman) filter, which was wrapped in a piece
131 of aluminum foil and kept at -20°C on board. Upon return to the lab, chlorophyll-*a*
132 samples were sonicated for 20 min and extracted in 5 ml 90% acetone at 4°C in the

133 dark for 24 hours. These samples were centrifuged at 4000 rpm for 10 min before
134 final determinations by standard fluorescence methods (Parsons et al., 1984) using a
135 Turner Designs Model 10 Fluorometer. [Concentrations of nitrate plus nitrite,](#)
136 [phosphate and silicate were determined by a Seal AA3 auto analyzer \(Bran-Lube,](#)
137 [GmbH\).](#) The low concentrations of nitrate plus nitrite and phosphate within the
138 euphotic zone were also determined by the long-cell method (Li et al., 2008; Li and
139 Hansell 2008) by incorporating a 50 cm liquid waveguide cell to AA3 with detection
140 limits of ~0.02 μM and ~0.01 μM , respectively.

141

142 2.2. Remote sensing observations

143 High-resolution satellite data, including sea surface temperature (SST), sea
144 surface chlorophyll (SSChl), surface geostrophic currents, as well as surface wind
145 stresses and Ekman velocities, were used to assess the spatial change of these surface
146 properties in the nSCS during the study period. Monthly averaged sea surface
147 chlorophyll- a ($0.04^\circ \times 0.04^\circ$) was acquired from the NASA's Moderate Resolution
148 Imaging Spectroradiometer data observed by the Aqua Satellite (MODIS-Aqua). Near
149 real time geostrophic currents ($0.2^\circ \times 0.2^\circ$) were from the NOAA's CoastWatch data
150 based on the daily sea level height anomaly and a climatological mean dynamic
151 height field by NOAA/AOML. Daily sea surface temperature ($0.1^\circ \times 0.1^\circ$) was acquired
152 from the NOAA's Geostationary Operational Environmental Satellite –Polar
153 Operational Environmental Satellite program (GOES-POES). Daily Ekman upwelling
154 velocities and surface wind stresses with a resolution of $0.25^\circ \times 0.25^\circ$ were derived
155 from the Advanced Scatterometer data by the European Meteorological and
156 Operational satellite program (METOP-ASCAT). The Ekman pumping velocity (w_e ,
157 negative for downwelling) at the depth of Ekman layer is calculated as (Gill, 1982)

$$158 \quad w_e = \frac{1}{\rho_w} \left(\nabla \times \frac{\tau}{f} \right) \quad (1)$$

159 where ρ_w is the density of seawater, which is assumed constant at 1024 kg m^{-3} ; f is the
160 Coriolis parameter; τ is the vector of wind stress.

162

163 2.3 Thorpe-scale analyses and vertical diffusivity

164 We applied a Thorpe-scale based approach (Thorpe 1977; Galbraith and Kelley

165 1996; Gargett and Garner 2008; Li et al., 2012) to estimate fine structure and
 166 turbulent diffusivity for each station using CTD downcast data. The method combines
 167 several criteria to determine the real overturns from a density profile (Li et al., 2012),
 168 including the test of minimum thickness, the run-length and water mass tests
 169 (Galbraith and Kelley 1996), as well as the tests of minimal overturn ratio and
 170 maximal T/S tightness (Gargett and Garner 2008). These criteria ensure that the
 171 maximal density difference within an overturn is greater than twice the measurement
 172 noise (0.001 kg m^{-3}). The length scale of an overturn is larger than twice the vertical
 173 resolution (Nyquist theorem) and larger than a minimum thickness (Galbraith and
 174 Kelley 1996). The percentage of positive/negative displacements within an overturn
 175 (the overturn ratio) is larger than 0.2 and the deviations on a T/S diagram are less than
 176 0.003 (Gargett and Garner 2008). The vertical resolution of CTD sampling during the
 177 cruise was $\sim 10 \text{ cm}$ with a fall rate of $\sim 2.4 \text{ m s}^{-1}$. Therefore, only overturns larger than
 178 0.5 m are included, to obtain five data point resolution. We discard data in the upper
 179 10 m , as the Thorpe approach is not strictly valid there. Once an overturn is identified,
 180 the Thorpe scale (L_T) is calculated from the root mean square of the vertical
 181 displacement (d_z) as $L_T = (\sum d_z^2)^{0.5}$.

182 Turbulent kinetic energy dissipation rate (ε) is calculated from L_T and N by

$$\varepsilon = 0.64 \cdot L_T^2 \cdot N^3 \quad (2)$$

183 where N is the buoyancy frequency given by $N^2 = -g\rho_0^{-1}(\partial\rho/\partial z)$ with g the
 184 gravitational acceleration, ρ_0 the mean density, and $\partial\rho/\partial z$ the density gradient across
 185 each overturn (Galbraith and Kelley 1996). According to Osborn (1980), the vertical
 186 diffusivity (K_z) can be estimated from ε and N by

$$K_z = 0.2 \cdot \varepsilon \cdot N^{-2} \quad (3)$$

187 The diffusive nutrient fluxes at the depth of interest can be estimated by multiplying
 188 the diffusivity (K_z) by the local nutrient gradient ($\partial C/\partial z$). Nutrient gradient, at the
 189 depth of Z_i with the concentration of C_i , is approximately estimated by
 190 $(C_{i+1} - C_i)/(Z_{i+1} - Z_i)$, with C_{i+1} the concentrations at Z_{i+1} immediately next to Z_i .

191
 192
 193
 194
 195
 196 2.4 Setup of dilution experiments

197 Phytoplankton growth and microzooplankton grazing in the surface waters of
 198 stations A and B near the edge of continental shelf were assessed on board using
 199 dilution technique (Landry and Hassett 1982; Landry et al., 1998; Li et al., 2011) on
 200 May 13th and May 17th, 2014. All the bottles, tubing and carboys were soaked in 10%
 201 (v/v) hydrochloric acid solution for over 24 hours and they were rinsed several times
 202 with deionized water and seawater before each experiment. Surface seawater,
 203 collected by an acid-washed polyethylene bucket, was screened through a 200- μ m
 204 mesh before being transferred into polycarbonate carboys as raw seawater. A dilution
 205 series was prepared with 0%, 25%, 50%, 75%, and 100% unfiltered seawater in
 206 duplicated polycarbonate bottles (0% unfiltered seawater sample was not performed at
 207 station B). Measured amounts of particle-free seawater, obtained by filtering the raw
 208 seawater with 0.45 μ m filters, were added to 2.4-liter polycarbonate bottles. These
 209 samples were then enriched with additional nutrients to promote constant growth of
 210 phytoplankton. Finally, each bottle was gently filled with unfiltered seawater to its
 211 capacity. There was also one bottle filled with 100% unfiltered raw seawater without
 212 nutrient enrichment to serve as the control for our experiment. All the bottles were
 213 tightly capped and incubated for 24 hours in a deck incubator, which was covered
 214 with a neutral density screen to mimic the natural sunlight and filled with flowing
 215 seawater from the sea surface to control the temperature. Duplicate 300 ml samples
 216 were taken from each bottle before and after the dilution experiments for
 217 chlorophyll- α measurements.

218 Specific rates of nutrient-saturated phytoplankton growth (μ_n , d^{-1}) and
 219 microzooplankton grazing (g , d^{-1}) are estimated by least-square regression between
 220 the net growth rates (η , d^{-1}) and the dilution factors (D) as

$$221 \eta = \frac{1}{t} \ln \left(\frac{P_t}{P_0} \right) = \mu_n - D \cdot g$$

222 (4)

223 where P_0 and P_t are the initial and final concentrations of chlorophyll- α , respectively
 224 and t is the duration of the incubation. The natural phytoplankton growth rate (μ),
 225 which is often subjected to nutrient limitation (Landry et al., 1998), is finally
 226 estimated from the net growth rate of raw seawater without nutrient enrichment (η_{raw})
 227 by $\mu = \eta_{raw} + g$.

228 To examine the response of the phytoplankton community to nutrient enrichment,

229 two bottles of raw seawater with nutrient additions were incubated for 4 days, with
230 chlorophyll-*a* and nutrient samples taken at the very beginning and each day
231 afterwards. Nutrient data within the exponential growth phase is used to estimate the
232 specific net nutrient consumption rate (*m*) of the incubated community by linear
233 regression of $\ln(C)$ and *t* assuming

$$\frac{dC}{dt} = -m \cdot C$$

235 (5)

236 where *C* is the concentration of dissolved nutrients in the sample.

237

238 3. Results

239 3.1 Hydrographic dynamics of the nSCS

240 During the survey of May 2014, waters of the nSCS can be grouped into three
241 regions (Fig. 1): the coastal ocean zone (stations C₁₋₆), the offshore pelagic zone
242 (stations C₇₋₁₀), and the water-intrusion zone near the Luzon Strait (stations C₁₁₋₁₃).
243 These three different zones were influenced by a diverse set of physical processes.
244 The coastal ocean zone, which can be further separated into two subregions including
245 the nearshore area (stations C₁₋₂) and the continental shelf (stations C₃₋₆), was strongly
246 affected by wind-driven upwelling processes including Ekman transport and Ekman
247 pumping (Gan et al., 2010). The nearshore area was characterized by low sea surface
248 temperature (Fig. 2a) as a result of upwelling via Ekman transport driven by
249 southwest monsoon along the shore. Ekman pumping induced by wind stress curl
250 showed a significant increase near the edge of the continental shelf far away from the
251 coastline (Fig. 2b). Upward transport of the deeper water with lower temperature but
252 higher salinity along the shelf slope was clearly seen during the transect (Fig. 3a and
253 3b), which could be a result of direct upwelling or alongshore advection of upwelled
254 waters from upstream. Both the offshore pelagic zone and the water-intrusion zone are
255 far from the coast with bottom depths more than 2000 m (Fig. 1). The offshore pelagic
256 zone was relatively stable with weak surface geostrophic currents, while the
257 water-intrusion zone was strongly influenced by Kuroshio intrusion through the
258 Luzon Strait (Fig. 2a).

259 Sea surface temperature from satellite showed a generally increasing trend from
260 the coastal regions near Shantou to the offshore regions near Luzon Strait due to the
261 decreasing latitude (Fig. 2a). The observed cross-shelf gradient of surface temperature

262 from the discrete bottle measurements is in good agreement with the satellite SST
263 data, with an average of 24.0 ± 0.6 °C near the coast, 25.2 ± 0.2 °C on the continental
264 shelf, 28.4 ± 0.5 °C in the offshore pelagic zone, and 29.1 ± 0.5 °C near the Luzon
265 Strait (Fig. 3a). Surface salinity was less variable than temperature from nearshore to
266 offshore with a difference of less than 0.3 during the survey (Fig. 3b). Although there
267 was slightly higher surface salinity on the continental shelf (34.1 ± 0.1), the average
268 salinity concentration at the surface in the coastal ocean zone (33.9 ± 0.2) was
269 generally the same as those of the offshore pelagic zone (33.8 ± 0.1) and the
270 water-intrusion zone (33.9 ± 0.3). Substantially higher subsurface salinities within the
271 euphotic zone between the offshore pelagic zone and the water-intrusion zone (Fig. 3b)
272 could come from the upwelled Pacific waters southwest of Taiwan (Chao et al.,
273 1996).

274 Surface geostrophic current data (vectors of Fig. 2a) reveals that station B was
275 located at the edge of two eddies with southward surface flows. Directions of wind
276 stresses in the nSCS were generally southwest during the study period except two
277 regions where wind stress changed direction (vectors of Fig. 2b): one in the northwest
278 of Dongsha Islands with southerly winds and the other in the Luzon Strait with
279 westerly winds. There were several places of curl-driven upwelling in the offshore
280 deep-water regions, though the entire area was predominantly downwelling. Large
281 curl-driven upwelling ($>0.5 \times 10^{-5}$ m s⁻¹) was only observed near the edge of the
282 continental shelf over abrupt changes of bathymetry. Strong temporal variations of
283 Ekman pumping velocity (Fig. 2d) could be found in the coastal station of C₆ and the
284 offshore station of C₁₃. Though the vertical velocities by Ekman pumping during our
285 sampling duration of May 14th-16th, 2014 are relatively low, they are representative of
286 the entire spring intermonsoon period from May 8th to June 7th, 2014 with
287 substantially low wind intensity (Fig. 2d).

288

289 3.2 Spatial patterns of chlorophyll-*a* and nutrients in the nSCS

290 Sea surface chlorophyll-*a* in the nSCS during May 2014 was very high in the
291 coastal ocean zone – particularly in the near-shore regions – and decreased slightly on
292 the continental shelf (Fig. 2c). In contrast, there was generally low sea surface
293 chlorophyll-*a* in the large areas of the offshore pelagic zone and the water-intrusion
294 zone. Concentrations of the surface chlorophyll-*a* from discrete measurements during
295 our survey (Fig. 3c), varying from 0.04 to 0.92 µg L⁻¹, is in good agreement with the

296 satellite remote sensing data. In particular, surface chlorophyll-*a* along the section
297 shows a general seaward-decreasing trend from the costal regions of $0.72 \pm 0.36 \mu\text{g}$
298 L^{-1} to the offshore regions of $0.09 \pm 0.04 \mu\text{g L}^{-1}$, which is consistent with the decrease
299 of surface nitrate concentrations from $>1.0 \mu\text{mol L}^{-1}$ near coast to $<1.0 \mu\text{mol L}^{-1}$ in
300 offshore (Fig. 3d). **There was a surface chlorophyll patch ($\sim 0.3 \mu\text{g L}^{-1}$) found at**
301 **station C₁₁ between the offshore pelagic zone and the water-intrusion zone during the**
302 **transect study (Fig. 3c), which could result from a surface phytoplankton bloom**
303 **spreading from the southwest coast of Taiwan to the offshore regions of the central**
304 **nSCS (Fig. 2c).**

305 Phytoplankton chlorophyll-*a* was vertically well mixed in the coastal ocean zone,
306 with clear subsurface maxima of chlorophyll-*a* only found in the offshore pelagic
307 zone and the water-intrusion zone (Fig. 3c). The depth of the subsurface chlorophyll
308 maxima followed the $\sigma_0 = 23.5$ isopycnal, which became much shallower when
309 approaching the continental shelf from offshore. The vertical distribution of nutrients
310 along the section generally followed the isopycnal surfaces in the upper water column
311 (Fig. 3d-f), revealing the importance of physical control on upper ocean
312 biogeochemistry. **The observed uplifts of isopycnals as well as the depths of**
313 **chlorophyll maximum and nutricline at stations C₆, C₈, C₉, C₁₀, and C₁₂ are consistent**
314 **with positive upwelling velocities driven by wind stress curl (Fig. 2b). Interestingly,**
315 **there were substantially higher phosphate and silicate concentrations at depths of**
316 **$\sim 200 \text{ m}$ (across the $\sigma_0 = 25.5$ isopycnal) for both stations C₉ and C₁₁ in the offshore**
317 **regions, which could be due to either a horizontal or vertical injection event prior to**
318 **our survey. Elevated chlorophyll-*a* at station C₁₁ was accompanied by not only the**
319 **subsurface high nutrients but also the high salinity in the euphotic zone, suggesting**
320 **possible vertical and horizontal nutrient transports in the upper layer. Curiously, low**
321 **chlorophyll-*a* was found at station C₉, which showed the highest nutrient**
322 **concentrations and nutrient gradients. Along the density interval of $\sigma_0 = 25$ and $\sigma_0 = 26$**
323 **in the water-intrusion zone there was evidence for isopycnal mixing between the**
324 **high-nutrient nSCS waters and the adjacent waters of Luzon Strait with lower nutrient**
325 **but higher temperature/salinity.**

326

327 3.3 Vertical diffusivity and diffusive nutrient fluxes

328 Turbulent diffusivity estimated by Thorpe analyses varied substantially from the

edge of continental shelf to the west of Luzon Strait during May 2014 (Fig. 4). An overall averaged K_z of $2.5 \times 10^{-4} \text{ m}^2 \text{ s}^{-1}$ for the upper 300 m of the offshore deep-water stations is much higher than the oceanic background diffusivity of $10^{-5} \text{ m}^2 \text{ s}^{-1}$, but is comparable to the previous basin-scale estimates in the nSCS (Tian et al., 2009; Liu and Lozovatsky 2012). There were relatively high mean diffusivities of 3.6×10^{-4} and $3.3 \times 10^{-4} \text{ m}^2 \text{ s}^{-1}$ at stations C₈ and C₁₁, compared to $2.5 \times 10^{-5} \text{ m}^2 \text{ s}^{-1}$ of station C₉. Although the nitrate gradient at the base of euphotic zone in C₉ (0.12 mmol m^{-2}) was about twice of that in C₁₁ (0.06 mmol m^{-2}), its diffusive nitrate flux ($0.26 \text{ mmol m}^{-2} \text{ d}^{-1}$) was only about 15% of that in C₁₁. Our data reveals a general decreasing of mean diffusivity from $1.1 \times 10^{-3} \text{ m}^2 \text{ s}^{-1}$ of C₅ on the continental shelf, to $6.3 \times 10^{-4} \text{ m}^2 \text{ s}^{-1}$ of C₆ over the continental slope, and to $9.1 \times 10^{-5} \text{ m}^2 \text{ s}^{-1}$ of C₇ in the offshore pelagic zone. Yang et al. (2014) measured turbulent diffusivity along a short section near the edge of the continental shelf southwest of Taiwan using a microstructure profiler during May 2004 – about the same place as our stations C₅ to C₇ (Fig. 1). Their results showed high turbulent mixing over the continental shelf with a mean diffusivity of $1.6 \times 10^{-3} \text{ m}^2 \text{ s}^{-1}$ but a much lower diffusivity of $5.2 \times 10^{-4} \text{ m}^2 \text{ s}^{-1}$ over the slope (Yang et al., 2014), which are well comparable with our estimates using Thorpe analyses.

Due to intermittent nature of the turbulence dissipation, the vertical structures of diffusivity observed during our study were quite patchy (Fig. 4). In order to investigate the vertical patterns of turbulent diffusivity, we compared the observations of the two incubation stations (stations A and B) with that of the reference time-series station S₁ (Fig. 5), which had a better vertical resolution of diffusivity. It is not surprising to find that the diffusivity profile of station A is quite similar to that of station S₁ (Fig. 5), as the two stations are very close to each other (Fig. 1). However, there are substantially higher diffusivities found in station B than in station S₁ (Fig. 5). The average diffusivity at 100 m during our study was about $1.6 \times 10^{-4} \text{ m}^2 \text{ s}^{-1}$ in station A but about $4.4 \times 10^{-4} \text{ m}^2 \text{ s}^{-1}$ in station B. The corresponding diffusive nitrate fluxes at the base of euphotic zone were thus about $0.65 \text{ mmol m}^{-2} \text{ d}^{-1}$ in station A and $3.03 \text{ mmol m}^{-2} \text{ d}^{-1}$ in station B, given their nitrate gradients of 0.05 and 0.08 mmol m^{-2} at 100 m, respectively (Table 1). [Region of the southeast Dongsha Islands near station B has been well documented for its high turbulent mixing because of internal waves and eddies \(e.g. Lien et al., 2005; Chow et al., 2008\)](#). Enhanced vertical mixing by nonlinear internal waves generated at the shelf edge near Dongsha Islands (Lien et al.,

362 2005) would lead to a higher surface chlorophyll- α and net primary production than
363 the adjacent areas with less influence of internal waves during the summertime (Pan
364 et al., 2012). **The high diffusivity and diffusive nitrate flux at station B may also be**
365 **contributed by physical dynamics associated with eddy-eddy interactions (Fig. 2a).**
366 The frontal zones at the edge of eddies are often places of increased vertical mixing
367 (Klein and Lapeyre 2009; Li et al., 2012), though the eddy-induced vertical fluxes
368 may vary substantially between cyclonic, anticyclonic and mode-water eddies
369 (McGillicuddy et al., 2007).

370

371 3.4 Rates of phytoplankton growth, microzooplankton grazing, and specific nutrient
372 consumption

373 Hydrographic and biogeochemical conditions of the two incubation stations were
374 quite different, with much higher temperature (Fig. 6) and salinity (data not shown)
375 but lower nutrients and nutrient gradients in station A than in station B (Fig. 6).
376 Station A was at the edge of a surface phytoplankton bloom (Fig. 2c) spreading from
377 the southwest coast of Taiwan to the offshore pelagic regions, while station B was
378 near the central nSCS with very low sea surface chlorophyll- α ($<0.1 \mu\text{g L}^{-1}$). Except
379 for the surface layer, chlorophyll- α concentration of station B was generally much
380 higher than that of station A throughout the water column. There was a clear
381 subsurface chlorophyll maximum of $\sim0.4 \mu\text{g L}^{-1}$ at 50 m for station B (Fig. 6), while
382 double peaks of chlorophyll- α were found for station A with a surface maximum of
383 $\sim0.3 \mu\text{g L}^{-1}$ and a subsurface maximum of $\sim0.1 \mu\text{g L}^{-1}$ at 75 m.

384 Rates of phytoplankton growth and microzooplankton grazing at the surface were
385 substantially different between the two stations. The nutrient-saturated phytoplankton
386 growth rate was 1.24 d^{-1} at station B, which was about three times of that at station A
387 (0.44 d^{-1}). On the other hand, the microzooplankton grazing rate of 0.43 d^{-1} at station
388 A was only slightly lower than the grazing rate of 0.60 d^{-1} at station B (Fig. 7). The
389 natural growth rate of phytoplankton, after correction for the effects of nutrient
390 enrichment as described in section 2.3, was 0.28 d^{-1} at station A, much lower than the
391 rate of 1.18 d^{-1} in station B. The rates measured at station B during May 2014 are
392 comparable with previous estimates of growth rates of 1.03 d^{-1} and grazing rates of
393 0.62 d^{-1} near Dongsha Islands during July 2009 (Chen et al., 2013). Our results for
394 station A are also in good agreement with those found in the non-upwelling area of the

395 south Taiwan Strait (Huang et al., 2011), which suggested mean rates of 0.4-0.5 d⁻¹
396 and 0.3-0.7 d⁻¹ for phytoplankton growth and microzooplankton grazing during July
397 2004 and 2005.

398 Incubation experiments in station A revealed an exponential growth of
399 phytoplankton chlorophyll-*a* in response to nutrient addition within the first two days,
400 before reaching a stable growth phase on the third day and a decay phase on the fourth
401 day; the chlorophyll-*a* of the control experiment with raw seawater without nutrient
402 additions quickly decreased as nutrients were consumed in the bottles (Fig. 8a). In
403 contrast, phytoplankton of station B showed no response to nutrient enrichment within
404 the first two days of incubation compared to the control experiment (Fig. 8b).
405 Significant increase of incubated chlorophyll-*a* for station B was only found during
406 the last two days of experiment (Fig. 8b). Nutrient utilization during
407 nutrient-enrichment incubations at these two stations were also quite different, with a
408 much slower specific rate of nutrient consumption at station B (0.46 d⁻¹) than at
409 station A (1.03 d⁻¹). These results suggest that there was stronger nutrient limitation of
410 the phytoplankton community at station A than station B during our cruise.

411

412 **4. Discussion**

413 4. 1 Roles of turbulent mixing and curl-driven upwelling on nutrient fluxes of the
414 nSCS during the spring inter-monsoon transition period

415 If the horizontal and atmospheric inputs are ignored, the total nutrient flux into the
416 euphotic zone (J_{total}) is the sum of diffusive flux due to turbulent dissipation
417 ($J_{dif}=K_z \partial C / \partial z$) and the advective flux due to upwelling ($J_{upw}=wC$, negative for
418 downwelling):

$$419 J_{total} = K_z \frac{\partial C}{\partial z} + wC$$

420 (6)

421 To assess the roles of turbulent diffusion and Ekman pumping on vertical transport of
422 nutrients in the nSCS, the diffusive and advective nitrate fluxes at the base of euphotic
423 zone was estimated from the continental shelf to the open sea during May 2014 (see
424 Table 1 for details). Vertical velocity (w) at the base of euphotic zone is assumed
425 equal to the curl-driven upwelling/downwelling velocity (w_e) by Ekman pumping. We
426 have neglected Ekman transport as its effect is restricted only to the near coast (Gan et
427 al., 2010). Variations of w during the transect study is consistent with the isopycnal

428 oscillation along the section (Fig. 3), suggesting the important role of Ekman pumping
429 on physical dynamics of the water column. At the continental slope of station C₆, the
430 vertical nitrate fluxes were largely supported by curl-driven upwelling, with turbulent
431 mixing playing a minor role due to low nitrate gradients. In contrast, the diffusive
432 nitrate flux was over three times of the upwelled nitrate flux at station C₇,
433 immediately adjacent to C₆. Except for station C₁₂, curl-driven downwelling was
434 observed in the deep-water regions during the transect study, leading to downward
435 transport of the low-nutrient surface water to the deeper layer. The upward nitrate
436 fluxes in these stations were thus determined by the intensities of diffusive fluxes
437 working against the downwelling fluxes. There was a negative nitrate flux found at
438 station C₉ where downwelling was stronger than the upward diffusion, resulting in a
439 loss of nitrate from the euphotic zone. Our findings suggest that it is the interplay of
440 turbulent diffusion and curl-driven upwelling/downwelling that controls the vertical
441 fluxes of nutrients into the euphotic zone to support phytoplankton production in the
442 nSCS.

443 For the deep-water stations including the offshore pelagic zone and the water
444 intrusion zone, the integrated chlorophyll-*a* biomass during the transect study shows a
445 positive correlation with the upward nitrate flux ($[Chl \cdot dz] = 16.75 \times J_{total} + 7.7$, $r^2 = 0.58$,
446 $p = 0.014$) when stations C₉ is not included (Table 1), supporting the important role of
447 bottom-up control on phytoplankton production in our study area (Chen 2005). From
448 the slope of 16.75, we could estimate a specific new production by vertical nitrate
449 supply of 0.060 molN (gChl)⁻¹ d⁻¹, which is slightly lower than 0.063-0.088 molN
450 (gChl)⁻¹ d⁻¹ reported in the nSCS by Chen (2005). Assuming a vertically constant rate
451 of phytoplankton specific growth, a gram chlorophyll-to-carbon ratio of 0.03 and a
452 molar C/N ratio of 6.625, we estimate a vertically integrated primary production of
453 ~12.3 mmolN m⁻² d⁻¹ in station B and ~1.8 mmolN m⁻² d⁻¹ in station A. The
454 contribution of vertical nutrient fluxes to primary production could thus be ~11% and
455 ~26% in stations B and A, respectively, which are comparable with the *f*-ratio of
456 0.14-0.20 previously estimated in the nSCS from late March to October (Chen, 2005).
457 In steady status, the net primary production of phytoplankton should be balanced by
458 the upward nutrient flux as well as the downward particle flux. Therefore, a high
459 nutrient flux would correspond to a high net primary production and thus a high
460 biomass accumulation, if other conditions remain the same (species, temperature,

461 light, grazing, etc). Station C₉ is interesting in that the vertical nutrient fluxes are net
462 downward out of euphotic zone, suggesting that the station may not be in steady
463 status. High nutrients here are likely a result of strong horizontal input or a previous
464 diapycnal nutrient injection. In this case, large drawdown of nutrients will be expected
465 by fast growing phytoplankton and by the downward transport of nutrients out of
466 euphotic zone.

467 Uncertainty of the vertical nutrient flux could be contributed by errors in the
468 determinations of vertical diffusivity and vertical velocity, as well as nutrient
469 concentration and gradient. Calculation errors of vertical diffusivity by the
470 Thorpe-scale approach, estimated from the time-series station S₁, were $0.87 \times 10^{-4} \text{ m}^{-2}$
471 s^{-1} at 50 m (n=5), $0.71 \times 10^{-4} \text{ m}^{-2} \text{ s}^{-1}$ at 100 m (n=6), and $0.46 \times 10^{-4} \text{ m}^{-2} \text{ s}^{-1}$ at 150 m
472 (n=7). We therefore obtain an average of $0.68 \times 10^{-4} \text{ m}^{-2} \text{ s}^{-1}$ for the overall uncertainty
473 of diffusivity determined in our study. Uncertainty of vertical velocity by Ekman
474 pumping from satellite observations could be approximately determined at each
475 station by their standard deviations over the sampling duration of May 14th-16th, 2014.
476 Measurement errors of nutrients at depths during the field study should be negligible
477 as the concentrations are considerably higher than the detection limits of the analytical
478 methods. We are not able to quantify the uncertainty of nutrient gradient, as we have
479 only one cast for each station with reduced resolution below the euphotic layer.
480 Meanwhile, the nutrient gradient and related diffusive flux that we have calculated at
481 the base of euphotic zone could be interpreted as a mean value between the two
482 adjacent bottle depths (100-200 m). The final uncertainties for the vertical nutrient
483 fluxes are summarized in Table 1, which vary substantially from 0.10 to 0.98 mmol
484 $\text{m}^{-2} \text{ d}^{-1}$ for stations in the offshore regions.

485
486 4.2 Impact of growth-grazing dynamics on phytoplankton chlorophyll biomass in the
487 nSCS

488 Distributions of phytoplankton in the ocean are controlled by complex physical
489 and biological interactions. To assess the influence of growth-grazing dynamics on
490 phytoplankton chlorophyll-*a* biomass in the nSCS, two stations with distinct
491 biogeochemical settings and nutrient fluxes were selected for measurements of
492 phytoplankton growth and microzooplankton grazing rates. In addition, the
493 community response to nutrient enrichments at the two stations was assessed by

494 continuous incubations for up to four days. Previous studies indicates that surface
495 phytoplankton community in the southeast Dongsha Islands is dominated by both
496 diatom and picoplankton such as *Prochlorococcus*, while picoplankton with
497 negligible diatoms are found in the non-upwelling area south of the Taiwan Strait
498 during late spring and early summer (Yang 2009; Huang et al., 2011). Our results of
499 substantially high phytoplankton growth rates observed at station B southeast of
500 Dongsha Islands are in agreement with its high nutrient concentrations and nutrient
501 fluxes compared to station A south of Taiwan Strait. When released from the
502 constraints by nutrient limitation, phytoplankton community will be expected to shift
503 from dominance by picoplankton toward a higher relative abundance of larger
504 phytoplankton because of their higher intrinsic capacity for growth (Agawin et al.,
505 2000).

506 Percentage of the primary production consumed by microzooplankton can be
507 estimated by the ratio of microzooplankton grazing over phytoplankton growth (g/μ)
508 (Landry et al., 1998). High g/μ ratios (~1.5) at station A suggest an elevated role of the
509 microbial food web in the south Taiwan Strait, promoting nutrient recycling to support
510 further phytoplankton growth. Whereas, the relatively higher microzooplankton
511 grazing rate but lower g/μ ratio at station B may indicate a greater efficiency of carbon
512 export near the Dongsha Islands, as the greater loss of diatoms through sinking or
513 grazing by mesozooplankton in regions with high nutrient supply (Landry et al., 1998).
514 Natural growth of phytoplankton at station B was much higher than its grazing
515 mortality, leading to a large net growth rate (growth minus grazing) of 0.58 d^{-1} , which
516 is consistent with the high integrated chlorophyll biomass in this station. In contrast, a
517 negative net growth rate of -0.15 d^{-1} was found at station A as a result of higher
518 grazing pressure. The specific phosphate consumption rate of 1.03 d^{-1} at station A was
519 about twice of that at station B (0.46 d^{-1}) suggesting a larger nutrient demand at
520 station A. There was actually a faster response of phytoplankton to nutrient
521 enrichment at station A than at station B indicating a stronger nutrient limitation in the
522 south Taiwan Strait. The negative net community growth and the higher nutrient
523 consumption rate at station A are consistent with the spring phytoplankton bloom of
524 the southwest Taiwan observed in the satellite data (Fig. 2c) being in its decline phase.
525 Indeed, the area of the phytoplankton bloom decreased substantially within two weeks
526 and was not visible by the middle of June, 2014 (from weekly mean sea surface
527 chlorophyll-*a* data of MODIS Aqua) supporting the important role of grazing activity

528 on phytoplankton distribution in the nSCS.

529 In conclusion, we have conducted a preliminary study on vertical nutrient fluxes
530 and phytoplankton dynamics in the nSCS. Our results suggest that phytoplankton
531 patchiness in the nSCS during the spring inter-monsoon of May 2014 was mainly
532 controlled by vertical nutrient fluxes, which were driven by both turbulent diffusion
533 and wind stress curl-driven upwelling. Our results also revealed an increasing role of
534 turbulent diffusion but a decreasing role of curl-driven upwelling on vertical transport
535 of nutrients from the coastal ocean zones to the offshore pelagic zones in the nSCS.
536 Elevated nutrient fluxes observed near the Dongsha Islands were found to support
537 high new production leading to net growth of phytoplankton community, whereas the
538 low nutrient fluxes of the south Taiwan Strait resulted in a negative net community
539 growth leading to decline of a phytoplankton bloom. As the findings presented here is
540 limited by the very narrow area and the very short period of sampling time, future
541 studies may be improved by addressing the variability of vertical nutrient fluxes and
542 its relationship to phytoplankton dynamics on a much longer time scale over a much
543 broader area of the nSCS.

544

545 *Acknowledgements*

546 We are grateful to the captain and crew of the *R/V Shiyuan III* for their helps during
547 the field work. This work is supported by a startup fund from a National
548 Talent-Recruitment Program and a grant from the Chinese Academy of Sciences'
549 Strategic Pilot Project No.XDA110202014 (to QPL).

550 *References*

551 Abraham, E.R.: The generation of plankton patchiness by turbulent stirring, *Nature*, 391,
552 577-580, 1998.

553 Agawin, N.S.R., Duarte, C.M., and Agusti, S.: Nutrient and temperature control of the
554 contribution of picoplankton to phytoplankton biomass and production, *Limnol. Oceanogr.*,
555 45, 591-600, 2000.

556 Bombar, D., Dippner, J.W., Doan, H.N., Ngoc, L.N., Liskow, I., Loick-Wilde, N., and
557 Voss, M.: Sources of new nitrogen in the Vietnamese upwelling region of the South China Sea,
558 *J. Geophys. Res.*, 115, C06018, doi:10.1029/2008JC005154, 2010.

559 Centurioni, L.R., Niiler, P.P., and Lee, D.K.: Observations of inflow of Philippine Sea
560 surface water into the South China Sea through the Luzon Strait, *J. Phys. Oceanogr.*, 34,
561 113-121, 2004.

562 Chao, S.Y., Shaw, P.T., and Wu, S.Y.: Deep water ventilation in the South China Sea,
563 *Deep-Sea Res.*, I 43, 445-466, 1996.

564 Chen, B., Liu, H., Landry, M.R., Dai, M., Huang, B., and Sun, J.: Close coupling between
565 phytoplankton growth and microzooplankton grazing in the western South China Sea, *Limnol.*
566 *Oceanogr.*, 54, 1084-1097, 2009.

567 Chen, B., Zheng, L., Huang, B., Song, S., and Liu, H.: Seasonal and spatial comparisons
568 of phytoplankton growth and mortality rates due to microzooplankton grazing in the northern
569 South China Sea, *Biogeosciences*, 10, 2775-2785, 2013.

570 Chen, Y.L.: Spatial and seasonal variations of nitrate-based new production and primary
571 production in the South China Sea, *Deep-Sea Res.*, II, 52, 319-340, 2005

572 [Chow, C., Hu, J., Centurioni, L.R., and Niiler, P.P.: Mesoscale Dongsha cyclonic eddy in](#)
573 [the northern South China Sea by drifter and satellite observations, *J. Geophys. Res.*, 113,](#)
574 [C04018, doi:10.1029/2007JC004542, 2008.](#)

575 Cullen, J.J., Franks, P.J.S., Karl, D.M., and Longhurst, A.: Physical influences on marine
576 ecosystem dynamics, in: *The sea*, 12, Robinson, A.R., McCarthy, J.J., Rothschild, B.J. (eds),
577 John Wiley & Sons, New York, 297–336, 2002.

578 Davis, C.S., Flierl, G.R., Wiebe, P.H., and Franks, P.J.S.: Micropatchiness, turbulence and
579 recruitment in plankton, *J. Mar. Res.*, 43, 109-151, 1991.

580 Eppley, R.W., and Peterson, B.J.: Particulate organic matter flux and planktonic new
581 production in the deep ocean, *Nature*, 282, 677-680, 1979.

582 Farris, A., and Wimbush, M.: Wind-induced intrusion into the South China Sea, *J.*
583 *Oceanogr.*, 52, 771–784, 1996.

584 Galbraith, P.S., and Kelley, D.E.: Identifying Overtures in CTD Profiles, *J. Atmos. Ocean.*
585 *Tech.*, 13, 688–702, 1996.

586 Gan, J., Lu, Z., Dai, M., Cheung, A., Liu, H., and Harrison, P.: Biological response to

587 intensified upwelling and to a river plume in the northeastern South China Sea: A modeling
588 study, *J. Geophys. Res.*, 115, doi: 10.1029/2009jc005569, 2010.

589 Gargett, A. E., and Garner, T.: Determining Thorpe scales from ship-lowered CTD
590 density profiles, *J. Atmos. Ocean. Tech.*, 25, 1657–1670, 2008.

591 Gaube, P., Chelton, D.B., Strutton, P.G., and Behrenfeld, M.J.: Satellite observations of
592 chlorophyll, phytoplankton biomass, and Ekman pumping in nonlinear mesoscale eddies, *J.*
593 *Geophys. Res.*, 118, 6349-6370, doi:10.1002/2013JC009027, 2013.

594 Gill, A.E. (Eds.): *Atmosphere-Ocean Dynamics*, International Geophysics Series, 30,
595 Academic Press, London, 1982.

596 Han, A., Dai, M., Gan, J., Kao, S., Zhao, X., Jan, S., Li, Q., Lin, H., Chen, C., Wang, L.,
597 Hu, J. Wang, L., and Gong. F.: Inter-shelf nutrient transport from the East China Sea as a
598 major nutrient source supporting winter primary production on the northeaster South China
599 Sea shelf, *Biogeosciences*, 10, 8159-8170, 2013.

600 Huang, B., Xiang, W., Zeng, X., Chiang, K., Tian, H., Hu, J., Lan, W., and Hong. H.:
601 Phytoplankton growth and microzooplankton grazing in a subtropical coastal upwelling
602 system in the Taiwan Strait, *Cont. Shelf Res.*, 31, 48-56, 2011.

603 Kim, T.K., Lee, K., Duce, R., Liss, P.: Impact of atmospheric nitrogen deposition on
604 phytoplankton productivity in the South China Sea, *Geophys. Res. Letters*, 41(9), 3156-3162,
605 2013.

606 Klein, P., and Lapeyre, G: The oceanic vertical pump induced by mesoscale and
607 submesoscale turbulence, *Annu. Rev. Mar. Sci.*, 1, 351-375, 2009.

608 Landry, M.R., Brown, S.L., Campbell, L., Constantinou, J., and Liu, B.: Spatial patterns
609 in phytoplankton growth and microzooplankton grazing in the Arabian Sea during monsoon
610 forcing, *Deep-Sea Res.*, II, 45, 2353-2368, 1998.

611 Landry, M.R., and Hassett, R. P.: Estimating the grazing impact of marine
612 micro-zooplankton, *Mar. Biol.*, 67(3), 283-288, 1982.

613 Li, Q.P., Franks, P.J.S., and Landry, M.R.: Microzooplankton grazing dynamics:
614 parameterizing grazing models with dilution experiment data in the California Current
615 Ecosystem, *Mar. Ecol. Prog. Ser.*, 438, 59-69, 2011.

616 Li, Q.P., Franks, P.J.S., Ohman, M.D., and Landry, M.R.: Enhanced nitrate flux and
617 biological processes in a frontal zone of the California Current System, *J. Plankton Res.*, 34,
618 790-801, 2012.

619 Li, Q.P., and Hansell, D.A.: Nutrient distribution in baroclinic eddies of the oligotrophic
620 North Atlantic and inferred impacts on biology, *Deep-Sea Res.*, II, 55, 1291-1299, 2008.

621 Li, Q.P., Hansell, D.A., and Zhang, J.Z.: Underway monitoring of nanomolar nitrate plus
622 nitrite and phosphate in oligotrophic seawater, *Limnol. Oceanogr. Methods*, 6, 319-326, 2008.

623 Li, Q.P., Wang, Y., Dong, Y., and Gan, J.: Modeling long-term change of planktonic

624 ecosystems in the Northern South China Sea and the upstream Kuroshio Current, *J. Geophys.*
625 *Res.*, 120, doi:10.1002/2014JC010609, 2015

626 Lien, R., Tang, T., Chang, M., and D'Asaro, E.A.: Energy of nonlinear internal waves in
627 the South China Sea, *Geophys. Res. Lett.*, 32, L05615, doi:10.1029/2004GL022012, 2005.

628 Lin, I., Lien, C., Wu, C., Wong, G.T.F., Huang, C., and Chiang, T.: Enhanced primary
629 production in the oligotrophic South China Sea by eddy injection in spring, *Geophys. Res.*
630 *Letters*, 37, L16602, doi:10.1029/2010GL043872, 2010.

631 Lin, I., Wong, G.T.F., Lien, C., Chien, C., Huang, C., and Chen, J.: Aerosol impact on the
632 South China Sea biogeochemistry: an early assessment from remote sensing, *Geophys. Res.*
633 *Letters*, 36, L17605, doi:10.1029/2009GL037484, 2009.

634 Liu, K.K., Chao, S.Y., Shaw, P.T., Gong, G.C., Chen, C.C., and Tang, T.Y.:
635 Monsoon-forced chlorophyll distribution and primary production in the South China Sea:
636 observations and a numerical study, *Deep-Sea Res., I*, 49, 1387-1412, 2002.

637 Liu, X., Furuya, K., Shiozaki, T., Masuda, T., Kodama, T., Sato, M., Kaneko, H.,
638 Nagasawa, M., and Yasuda, I.: Variability in nitrogen sources for new production in the
639 vicinity of the shelf edge of the East China Sea in summer, *Cont. Shelf Res.*, 61-62, 23-30,
640 2013.

641 Liu, Z.Y., and Lozovatsky, I.: Upper pycnocline turbulence in the northern South China
642 Sea, *Chin. Sci. Bull.*, 57(18), 2302-2306, 2012.

643 McGillicuddy, D.J., Anderson, L., Bates, N., Bibby, T., Buesseler, K., Carlson, C., Davis,
644 C., Ewart, C., Falkowski, P., Goldthwait, S., Hansell, D.A., Jenkins, W.J., Johnson, R.,
645 Kosnyrev, V., Ledwell, J.R., Li, Q.P., Siegel, D.A., and Steinberg, D.K.: Eddy-wind
646 interactions stimulate extraordinary mid-ocean plankton blooms, *Science*, 316, 1021-1026,
647 2007.

648 Osborn, T.R.: Estimates of the local rate of vertical diffusion from dissipation
649 measurements, *J. Phys. Oceanogr.*, 10(1), 83-89, 1980.

650 Pan, X., Wong, G.T.F., Shiah, F.K., and Ho, T.Y.: Enhancement of biological production
651 by internal waves: observations in the summertime in the northern South China Sea, *J.*
652 *Oceanogr.*, 68, 427-437, 2012.

653 Parsons, T.R., Maita, Y., and Lalli, C.M. (Eds.): *A manual of chemical and biological*
654 *methods for seawater analysis*, Pergamum Press, Oxford, 1984.

655 Risien, C.M., and Chelton, D.B.: A global climatology of surface wind and wind stress
656 fields from eight year QuickSCAT scatterometer data, *J. Phys. Oceanogr.*, 38, 2379-2412,
657 2008.

658 Rykaczewski, R.R., and Checkley, D.M.: Influence of ocean winds on the pelagic
659 ecosystem in upwelling regions, *PNAS*, 105(6), 1065-1970, 2008.

660 Strom, S. L., Macri, E. L., and Olson, M. B.: Microzooplankton grazing in the coastal

661 Gulf of Alaska: Variations in top-down control of phytoplankton, Limnol. Oceanogr., 52,
662 1480–1494, 2007.

663 Tian, J., Yang, Q., and Zhao, W.: Enhanced diapycnal mixing in the South China Sea. J.
664 Phys. Oceanogr., 39, 3191-3203, 2009.

665 Thorpe, S.A.: Turbulence and mixing in a Scottish loch, Phil. Trans. Royal Soc., London
666 A, 286, 125–181, 1977.

667 Wang, J., and Tang, D.: Phytoplankton patchiness during spring intermonsoon in west
668 coast of South China Sea, Deep-Sea Res, II, 101, 120-128, 2014.

669 Yang, Q., Tian, J., Zhao, W., Liang, X., and Zhou, L.: Observations of turbulence on the
670 shelf and slope of northern South China Sea, Deep-Sea Res., I, 87, 43-52, 2014.

671 Yang, Y.H.: Phytoplankton community structure of the northern South China Sea and the
672 Philippine Sea, Master Thesis (in CHN), National Taiwan Normal University, Taiwan, 73 pp.,
673 2009.

674 Zhou, L., Tan, Y., Huang, L., Huang, J., Liu, H., and Lian, X.: Phytoplankton growth and
675 microzooplankton grazing in the continental shelf area of northeastern South China Sea after
676 typhoon Fengshen, Cont. Shelf Res., 31, 1663-1671, 2011.

677 Table 1: Comparisons of integrated chlorophyll-*a* ($\int Chl \cdot dz$), nitrate gradient ($\partial C/\partial z$),
678 nitrate concentration (NO_3), vertical diffusivity (K_z), upwelling velocity (w_e), diffusive
679 nitrate flux (J_{dif}), upwelled nitrate flux (J_{upw}), and total nitrate flux (J_{total}) for transect
680 stations C₆₋₁₂ and incubation stations A and B at ~1% light depth (~100m depth).

Station	$\int Chl \cdot dz$ [mg m ⁻²]	$\partial C/\partial z$ [mmol m ⁻⁴]	NO_3 [mmol m ⁻³]	^a K_z [10 ⁻⁵ m ² s ⁻¹]	^b w_e [10 ⁻⁵ m s ⁻¹]	J_{dif} [mmol m ⁻² d ⁻¹]	^c J_{upw} [mmol m ⁻² d ⁻¹]	J_{total} [mmol m ⁻² d ⁻¹]
C ₆	16.8	0.001	5.01	6.30±0.68	0.28±0.02	0.05±0.01	1.21±0.09	1.27±0.10
C ₇	20.2	0.077	6.42	0.91±0.68	0.03±0.05	0.60±0.45	0.17±0.27	0.77±0.73
C ₈	22.1	0.079	7.47	3.60±0.68	-0.21±0.08	2.44±0.46	-1.36±0.52	1.09±0.98
C ₉	15.4	0.122	9.52	0.25±0.68	-0.12±0.03	0.26±0.72	-0.99±0.25	-0.72±0.96
C ₁₀	21.7	0.082	9.37	3.45±0.68	-0.18±0.03	2.44±0.48	-1.46±0.24	0.99±0.72
C ₁₁	38.7	0.060	2.08	3.30±0.68	-0.27±0.07	1.71±0.35	-0.49±0.13	1.23±0.48
C ₁₂	20.7	0.029	3.93	1.53±0.68	0.05±0.05	0.39±0.17	0.17±0.17	0.56±0.34
C ₁₃	13.2	0.046	1.98	2.26±0.68	-0.27±0.17	0.91±0.27	-0.46±0.29	0.44±0.56
A	15.7	0.047	2.09	1.60±0.68	-0.09±0.04	0.65±0.28	-0.16±0.08	0.49±0.35
B	24.8	0.080	4.82	4.40±0.68	-0.41±0.11	3.03±0.47	-1.71±0.46	1.33±0.93

681

682 ^a uncertainty of K_z from Thorpe analyses is estimated as 0.68×10^{-4} m² s⁻¹ (see text for detail)

683 ^b w_e are 3-day-mean of May 14th-16th, 2014, except station B that is of May 12th-14th, 2014

684 ^c assuming vertical velocity at the depth of 100m is equal to w_e .

685 Figure 1: Sampling map in the northeastern South China Sea during May 2014. Dash
686 lines show the topography of the study area; solid dots are the stations for a transect
687 study (C₁₋₁₃) during May 14th-16th, 2014; star is a time-series reference station (S₁);
688 filled squares are two stations where shipboard dilution experiments were performed
689 (A and B). Inserted plot shows the temperature/salinity diagram for the transect with
690 arrows indicating waters from the coastal ocean zone (thick gray lines), the offshore
691 pelagic zone (thick black lines), and the Kuroshio intrusion zone (thin lines).

692
693 Figure 2: Spatial distributions of (a) sea surface temperature, (b) curl-driven
694 upwelling velocity, and (c) sea surface chlorophyll during the survey, together with (d)
695 the time-series of curl-driven upwelling and wind stress at stations C₆ and C₁₃ during
696 May-June, 2014. Vectors in panel (a) and panel (b) are surface geostrophic currents
697 and wind stresses, respectively; geostrophic current is from 3-day-mean altimetry data
698 from NOAA/AOML; upwelling velocity and wind stress are from 3-day mean
699 METOP-ASCAT data; sea surface temperature is 3-day-mean GOES-POES data; sea
700 surface chlorophyll-*a* is monthly MODIS-Aqua data.

701
702 Figure 3: Vertical distributions of (a) temperature [T], (b) salinity [S], (c)
703 chlorophyll-*a* [Chl-*a*], (d) nitrate [NO₃], (e) silicate [Si(OH)₄], and (f) phosphate [PO₄]
704 along the coastal transect of the northern South China Sea. Overlaid white lines in
705 each panel are isopycnals.

706
707 Figure 4: Profiles of Thorpe displacement (d_z), Thorpe scale (L_T), and turbulent
708 diffusivity (K_z) for nine stations (C₅, C₆, C₇, C₈, C₉, C₁₀, C₁₁, C₁₂, C₁₃) from the edge
709 of continental shelf to the west of Luzon Strait. Locations of these stations are shown
710 in Figure 1.

711
712 Figure 5: Comparisons of vertical turbulent diffusivities (K_z) between two stations A
713 and B. Black line is the result of the reference station S₁ with continuous CTD
714 sampling up to 13 casts; circles are for station A (2 casts) with squares for station B (2
715 casts).

716
717 Figure 6: Comparisons of vertical profiles of chlorophyll-*a* [Chl-*a*], temperature [T],
718 nutrients [Si(OH)₄, NO₃, PO₄], and nutrient gradients between two incubation stations
719 A and B. Thick lines in each panel are for bottom axis with thin lines (open symbols)
720 for top axis; dash lines are for station A with solid lines for station B.

721
722 Figure 7: Dilution experiment plots of phytoplankton net growth rates against the
723 dilution factors for stations A and B. Filled circles are net growth rates of the raw
724 seawater without nutrient enrichments.

725
726 Figure 8: Temporal variations of chlorophyll-*a* and phosphate during incubations with
727 and without nutrient enrichments in stations A and B. Dash lines (filled symbols) are
728 for chlorophyll-*a* in left axis with thin lines (open symbols) for phosphate in right axis;
729 control is the incubation of raw seawater without nutrient addition.

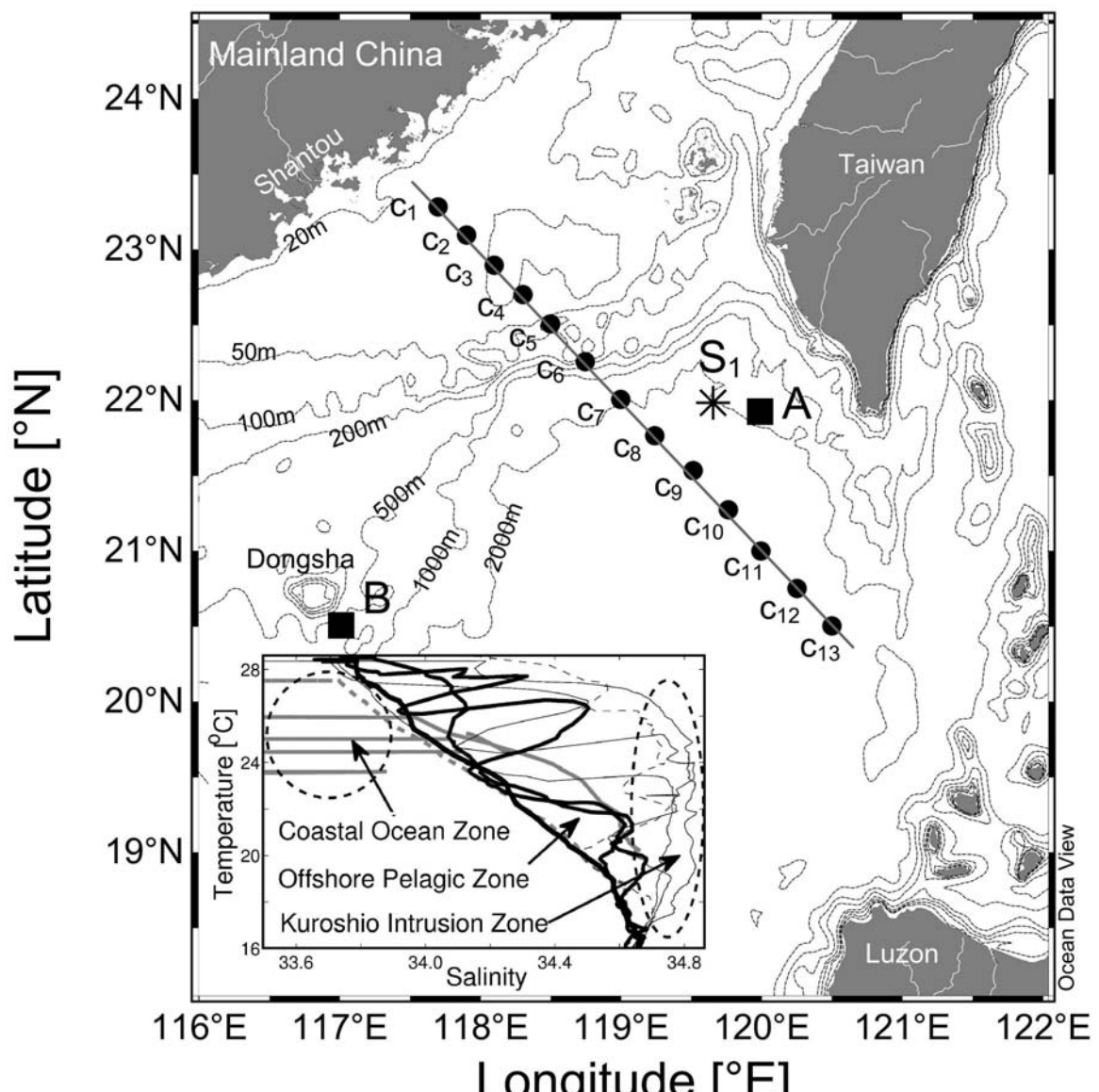
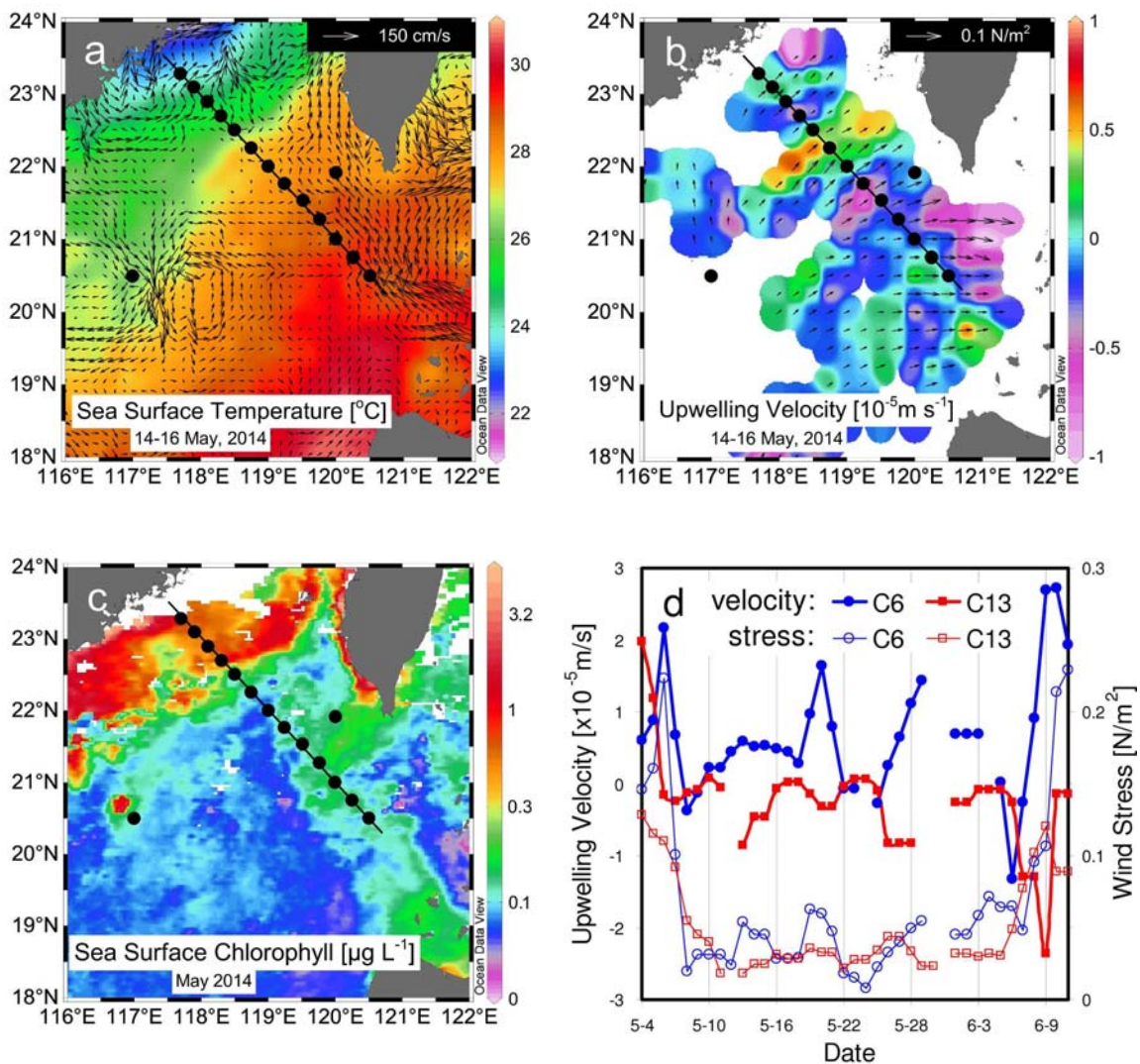


Figure 1

730
731
732



733
734
735

Figure 2

736

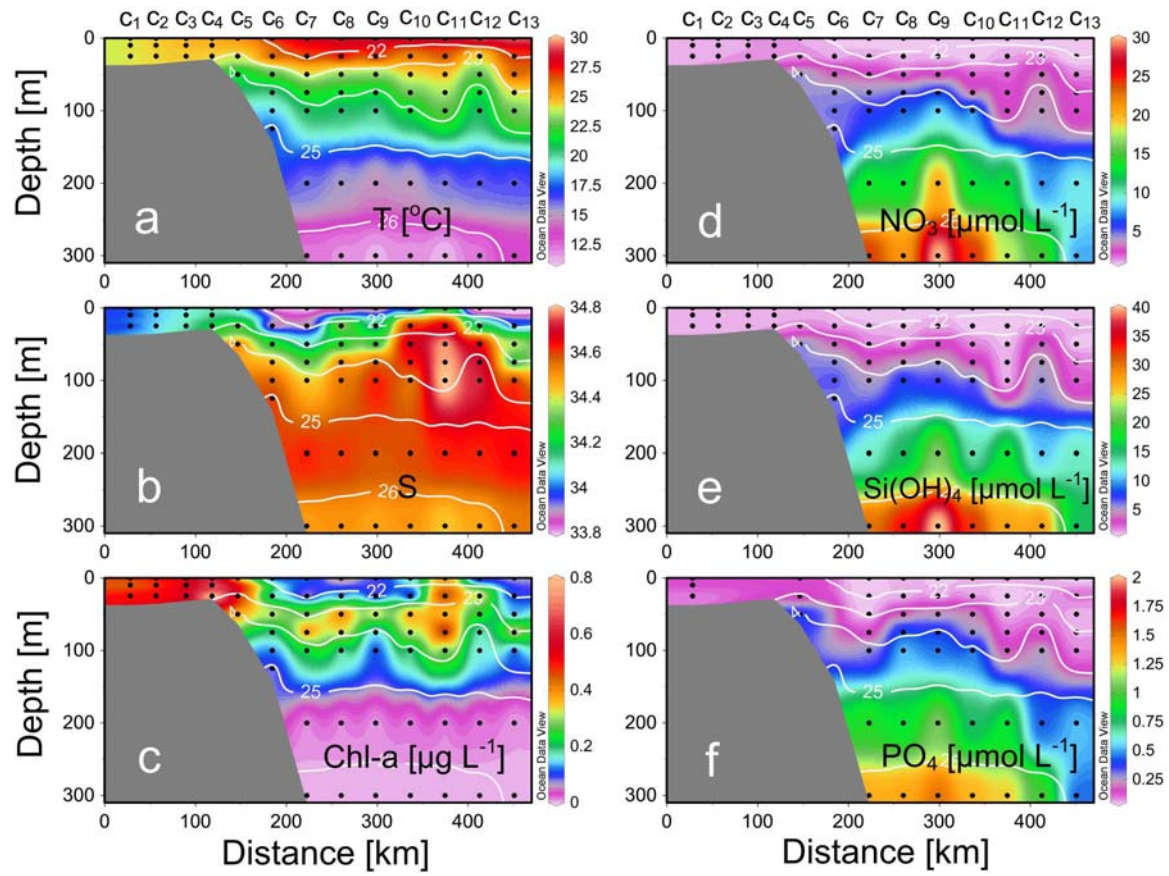
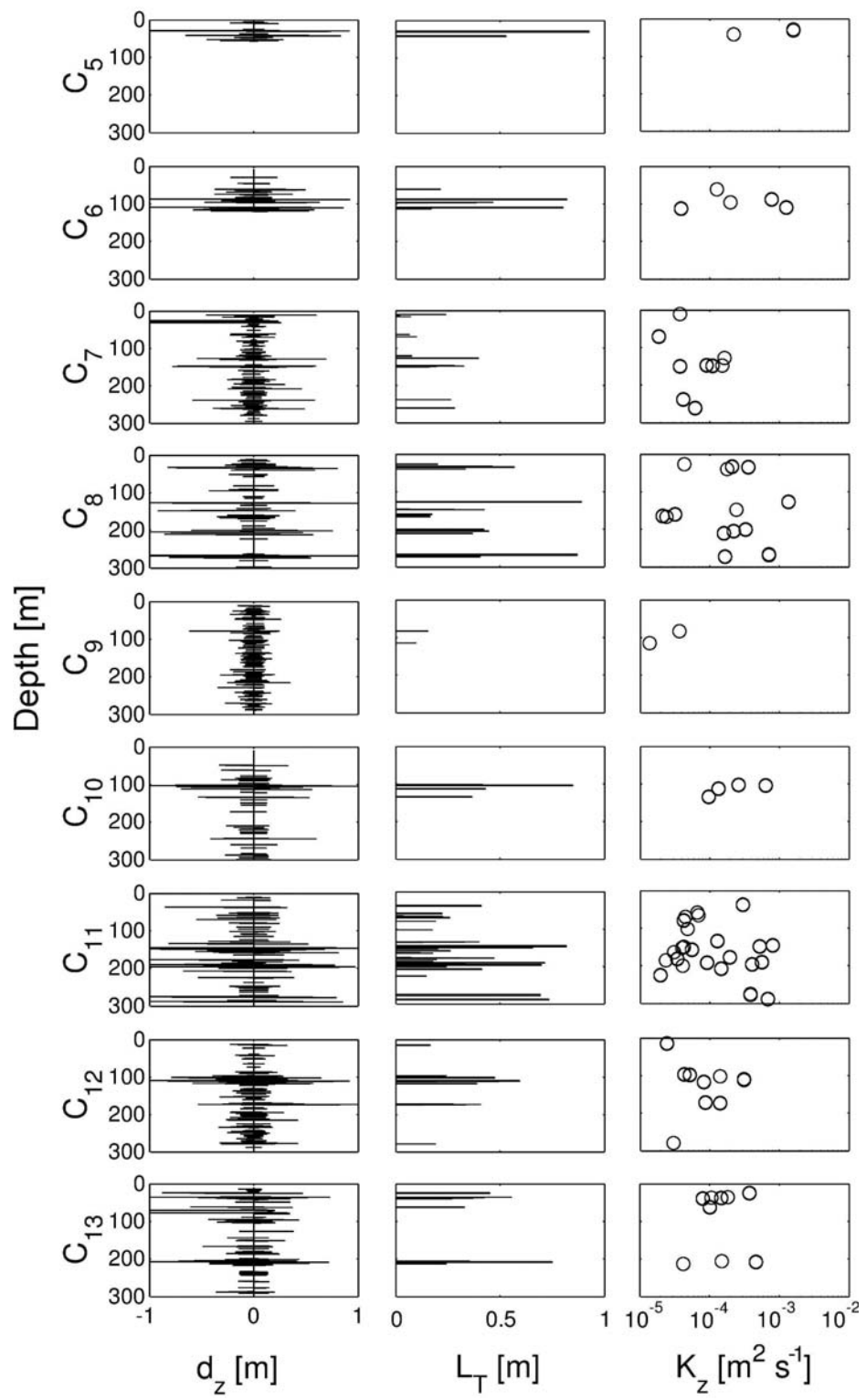


Figure 3

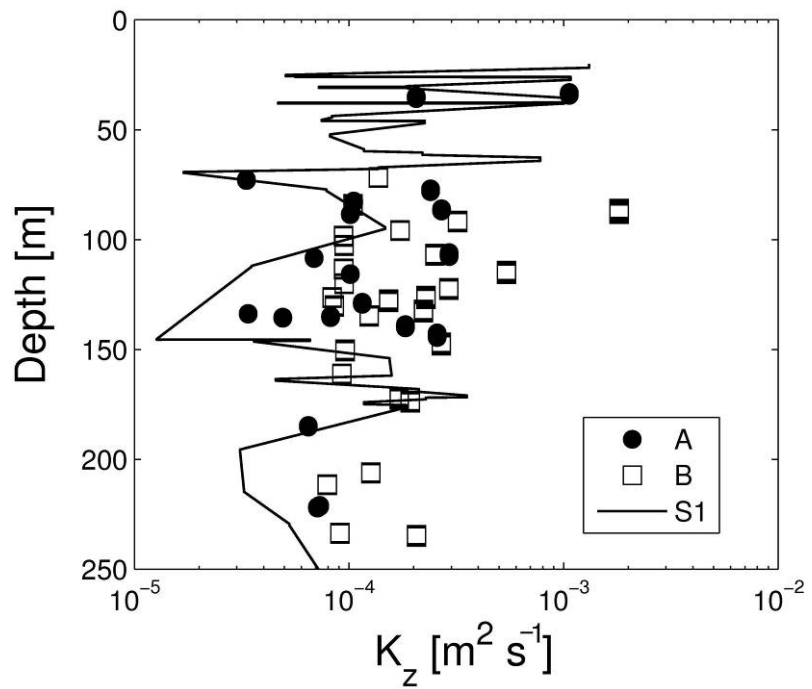
737

738



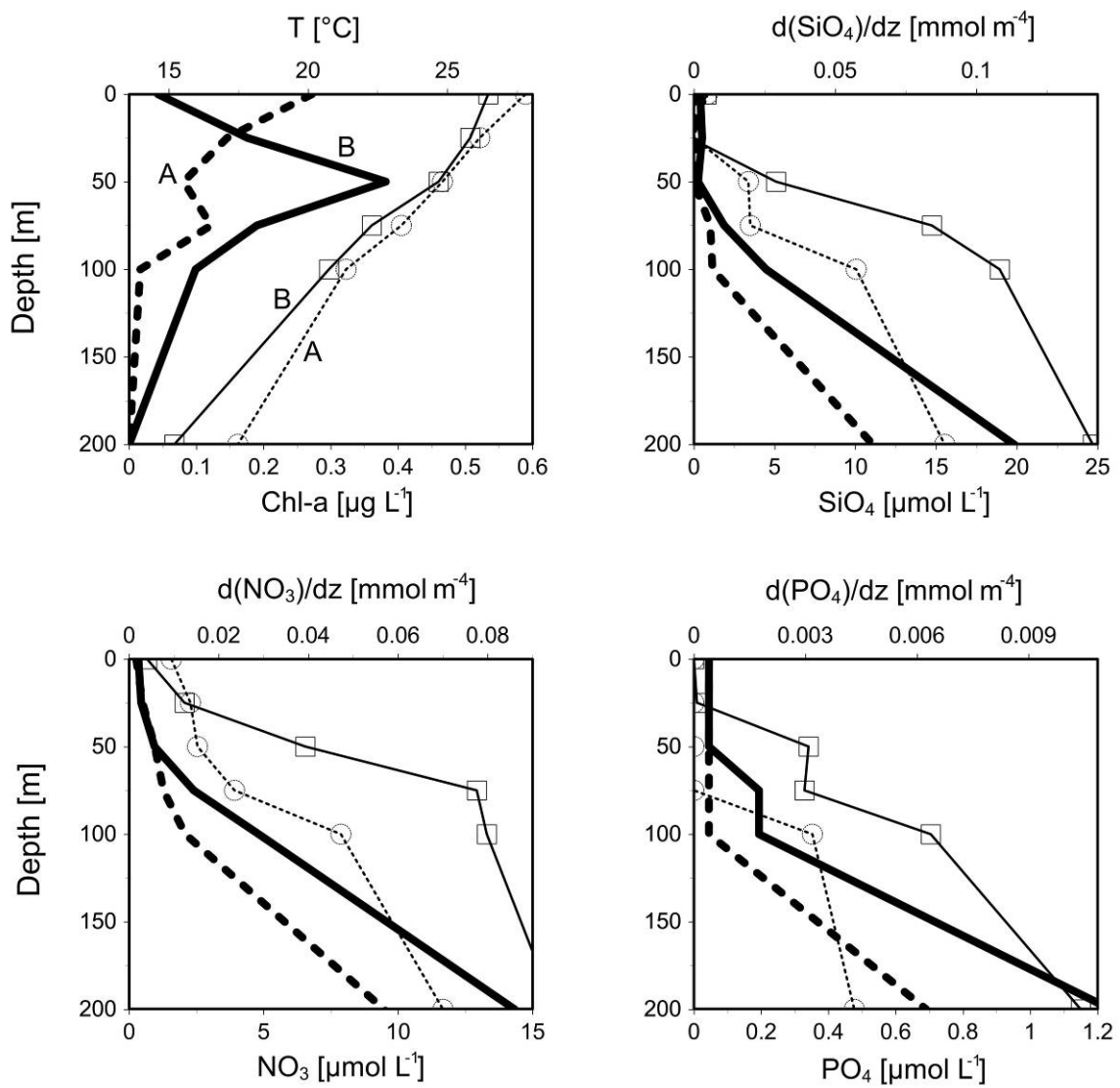
739
740
741

Figure 4



742
743
744

Figure 5



745
746
747

Figure 6

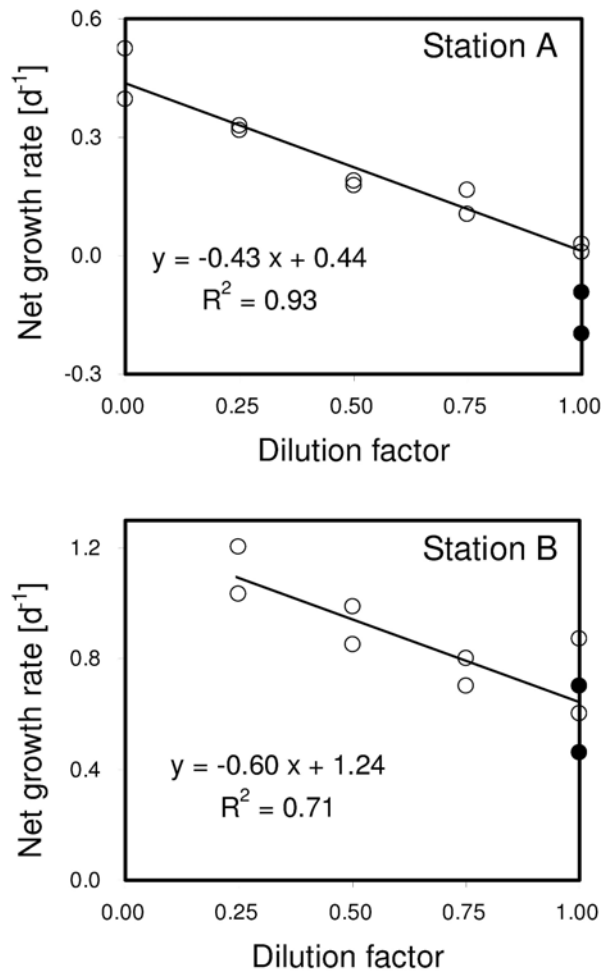


Figure 7

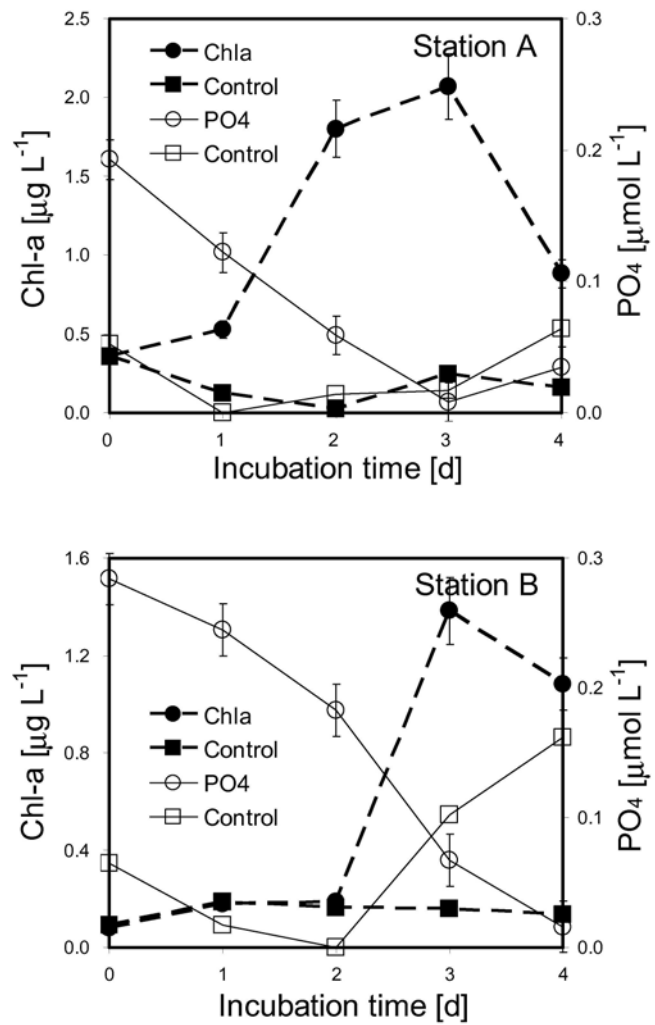


Figure 8